Drought and Deforestation: Has Land Cover Change Influenced Recent Precipitation Extremes in the Amazon?

JUSTIN E. BAGLEY*

Center for Sustainability and the Global Environment, and Department of Atmospheric and Oceanic Sciences, University of Wisconsin–Madison, Madison, Wisconsin

ANKUR R. DESAI

Department of Atmospheric and Oceanic Sciences, University of Wisconsin–Madison, Madison, Wisconsin

KEITH J. HARDING AND PETER K. SNYDER

Department of Soil, Water, and Climate, University of Minnesota, Twin Cities, St. Paul, Minnesota

JONATHAN A. FOLEY

Institute on the Environment, University of Minnesota, Twin Cities, St. Paul, Minnesota

(Manuscript received 20 June 2012, in final form 19 July 2013)

ABSTRACT

Expansion of agricultural lands and inherent variability of climate can influence the water cycle in the Amazon basin, impacting numerous ecosystem services. However, these two influences do not work independently of each other. With two once-in-a-century-level droughts occurring in the Amazon in the past decade, it is vital to understand the feedbacks that contribute to altering the water cycle. The biogeophysical impacts of land cover change within the Amazon basin were examined under drought and pluvial conditions to investigate how land cover and drought jointly may have enhanced or diminished recent precipitation extremes by altering patterns and intensity. Using the Weather Research and Forecasting (WRF) Model coupled to the Noah land surface model, a series of April–September simulations representing drought, normal, and pluvial years were completed to assess how land cover change impacts precipitation and how these impacts change under varied rainfall regimes. Evaporative sources of water vapor that precipitate across the region were developed with a quasi-isentropic back-trajectory algorithm to delineate the extent and variability that terrestrial evaporation contributes to regional precipitation. A decrease in dry season latent heat flux and other impacts of deforestation on surface conditions were increased by drought conditions. Coupled with increases in dry season moisture recycling over the Amazon basin by ~7% during drought years, land cover change is capable of reducing precipitation and increasing the amplitude of droughts in the region.

1. Introduction

Within the last 6 yr, the Amazon basin has experienced two once-in-a-century-level droughts. The impacts of the 2005 and 2010 droughts ranged from large increases in fire frequency and reduced river drainage rates to a reversal of the Amazon region from an estimated net sink of carbon from ~0.4 PgC yr^{-1} in normal years to a source of ~1.2 PgC yr^{-1} in 2005 and ~1.8 PgC yr^{-1} for 2010 (Phillips et al. 2009; Lewis et al. 2011). The droughts were extensive and affected approximately 1.9 million km^2 in 2005 and 3.0 million km^2 in 2010 (Phillips et al. 2009; Lewis et al. 2011). This work specifically addresses how current levels of tropical deforestation may have influenced recent drought severity and how the magnitude of impacts from land cover change are altered in drought relative to pluvial years.

Historically, major droughts in the Amazon basin have been correlated with modes of ocean temperature

* Current affiliation: Institute for Genomic Biology, University of Illinois at Urbana–Champaign, Urbana, Illinois.

Corresponding author address: Justin E. Bagley, Rm. 131D, Institute for Genomic Biology, 1206 West Gregory Dr., MC-195, Urbana, IL 61801.
E-mail: jbagley@illinois.edu

DOI: 10.1175/JCLI-D-12-00369.1

variability, particularly the El Niño–Southern Oscillation (ENSO) and Atlantic multidecadal oscillation (AMO). Droughts in the Amazon are typically associated with positive ENSO conditions in the Pacific Ocean (Grimm et al. 1998; Marengo 2004; Marengo et al. 2008; Yoon and Zeng 2010). However, the 2005 and 2010 droughts appear to have been driven primarily by record high sea surface temperature in the tropical North Atlantic (Marengo et al. 2011). Additionally, several studies have suggested that the Amazon basin is at particular risk of increased variability in rainfall regimes when confronted with the prospect of changing ocean temperatures from anthropogenic greenhouse gas emissions (Malhi et al. 2008; Grimm 2010).

Within the Amazon basin, there are distinct wet and dry seasons associated with the movement of the intertropical convergence zone and the establishment of the South American monsoon system (Nobre et al. 2009). In the southern Amazon, the dry season generally spans the July–September (JAS) months and the wet season occurs from January to March, although these dates are subject to some spatial and interannual variability, with the portion of the Amazon north of the equator having opposite seasonality (Fisch et al. 2004). During the wet season, climatological precipitation rates over the southern Amazon are $\sim$300 mm month^{-1}, while in the dry season the mean precipitation rate drops to $\sim$50 mm month^{-1}, with most of the moisture in the southern Amazon being supplied by intermittent weather systems (Fisch et al. 2004). As a result of this difference in precipitation, the impacts of droughts are most severe during the austral winter months, with both the frequency of late dry season precipitation and the magnitude of water deficit during this period contributing to the severity of the drought (Medvigy et al. 2011).

Accompanying interannual changes from sea surface variability and future climate change are the impacts of land cover change in the Amazon basin. As of 2003, approximately 15% of the Brazilian rain forest had been converted to a managed landscape (Soares-Filho et al. 2006; Alves et al. 2009). Much of this conversion of natural vegetation occurred on the southeastern edge of the rain forest, along the Mato Grosso border in an arc of rain forest deforestation. The arc of deforestation remains one of the most active regions in the world for the conversion of natural landscapes to managed systems, primarily for use as cattle pasture or soybean crops (Morton et al. 2006). In addition to altering a host of ecosystem services (Foley et al. 2007), there is extensive evidence that the conversion of tropical rain forest to pasture or cropland alters the hydrological cycle over a range of scales (Sahin and Hall 1996; Baidya Roy and Avissar 2002; Costa and Cardille 2003; D'Almeida et al. 2007; Costa and Pires 2010; Lee and Berbery 2012).

The impacts of tropical deforestation on the hydrological cycle are locally forced as high biomass trees with extensive root networks capable of accessing deep reservoirs of soil moisture are replaced with pasture or cropland. The biogeophysical impacts of this conversion on the surface energy balance includes a large reduction in latent heat flux, a small reduction in net radiation, and a moderate increase in sensible heat flux and surface energy storage (Gash and Nobre 1997; Fisch et al. 2004). This shift in the surface energy balance alters the atmospheric boundary layer, which can then influence regional or potentially global circulation and hydrology depending on the scale of the deforestation (Baidya Roy and Avissar 2002; Snyder et al. 2004; D'Almeida et al. 2007; Snyder 2010; Bagley et al. 2011). Additionally, surface runoff increases to balance the excess moisture, altering river flow (Costa and Cardille 2003; Coe et al. 2011).

Currently no scientific consensus exists on the regional impacts of deforestation on precipitation in the Amazon basin or on the response of vegetation to altered rainfall regimes within the region. Recent studies using satellite observations have been inconclusive on the vegetative response to drought in the region, with some suggesting ''greening-up'' of the Amazon due to reduced cloud cover under drought conditions (Huete et al. 2006; Saleska et al. 2007) and others refuting that claim (Brando et al. 2010; Xu et al. 2011). Meanwhile, modeling studies of the impacts of deforestation on precipitation have produced partially incongruent results, depending on both the scale of modeled deforestation and the resolution of the computational model (D'Almeida et al. 2007). In general, these studies have been carried out over either multiyear time scales with single column models or low-resolution general circulation models or short time scales (on the order of 1 week) with high-resolution mesoscale models (D'Almeida et al. 2007). Only a few seasonal-to-yearly time-scale, high-resolution modeling studies have been published (Walker et al. 2009; Medvigy et al. 2011; Lee and Berbery 2012).

In this study, we investigated the recent impact of drought and deforestation on the Amazon basin during the dry season using a state-of-the-art, high-resolution mesoscale model on a seasonal time scale. Specifically, we selected 6 yr between 2003 and 2010 that represented drought, normal, and pluvial precipitation regimes in the Amazon basin and modeled the impact that currently observed deforestation has on the surface energy balance, meteorological state, and precipitation in the region. We used quasi-isentropic back-trajectory analysis of water vapor based on the analysis of Brubaker et al.

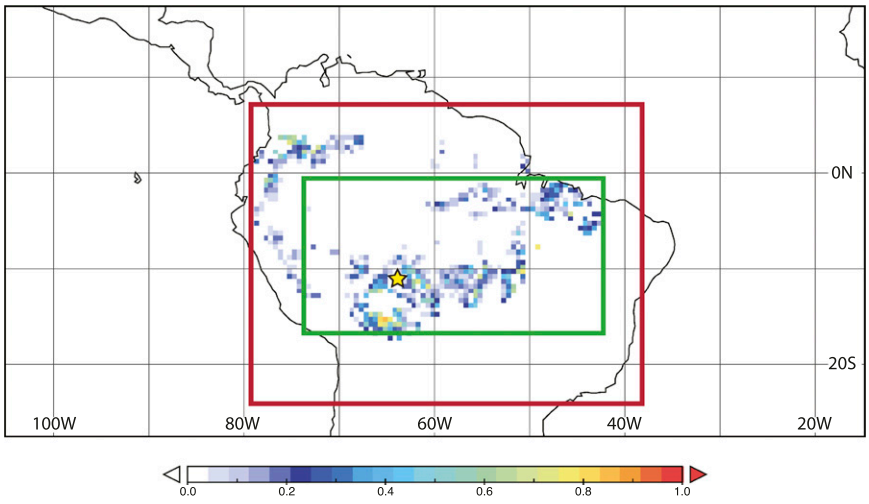

FIG. 1. The combined fractional land use for cropland and pastureland within the Amazon rain forest as defined by the potential vegetation dataset from Ramankutty and Foley (1999). The red box indicates the computational domain for the WRF-Noah simulations. Also shown is the region used for recycling calculations (green box). The starred location indicates the location of the paired ABRACOS–RBLE site used for surface flux comparison.

(2001) and Harding and Snyder (2012) to determine where moisture evapotranspired from deforested regions fell as precipitation and how the magnitude and pattern of this moisture changes with deforestation and natural variability. In this study we specifically address two questions: 1) Have current levels of tropical deforestation altered the severity and spatial distribution of recent severe droughts? and 2) How does the magnitude of recycled moisture in the southern Amazon basin change during years of extreme drought relative to pluvial years and how does deforestation impact moisture recycling?

2. Methods

a. Mesoscale model description, simulation parameters, and experimental design

The Weather Research and Forecasting (WRF) Model (version 3.2) coupled to the Noah land surface model was used to simulate the impacts of land cover change and varied rainfall regimes on the surface climate and regional hydrology for 6 yr between 2003 and 2010 (Skamarock et al. 2008). For each of the years 2003, 2004, 2005, 2007, 2009, and 2010, we conducted two simulations of the coupled WRF-Noah model. These years were selected based on a review of the literature, with 2005 and 2010 as extreme drought years, 2004 and 2009 as pluvial years, and 2003 and 2007 experienced normal conditions (Lewis et al. 2011; Marengo et al. 2011; Saatchi et al. 2012). Using vegetation and land use datasets described in section 2c, vegetation in the first simulation was set to potential vegetation over the Amazon basin. In the second simulation, potential vegetation was converted to pasture in regions where managed landscapes now comprise the dominant form of vegetation and a crop–forest mix in intermediate regions.

The WRF Model is a nonhydrostatic mesoscale model that has been implemented to fulfill both research and operational needs and has been coupled to the Noah model for land surface simulation. We applied the model with a 20 km $\times$ 20 km horizontal resolution over the Amazon basin and northern South America as shown in Fig. 1 (red box), with a 60-s time step and hourly output. Each model run was initialized on 15 March of a given year and run through 1 October to capture the months preceding and during the southern Amazon's dry season. By ending on 1 October, we reduced impacts of changes in dry season length due to deforestation that have been tested in other studies (e.g., Costa and Pires 2010) in order to focus on the direct changes to precipitation trajectories and moisture recycling effects. The first 15 days of the simulations were not used in the analysis to allow for model spin up. Initial and boundary conditions for meteorological, soil, surface, and sea surface temperature variables were provided from the National Centers for Environmental Prediction–U.S. Department of Energy (NCEP–DOE) Reanalysis 2 at T62 resolution every 6 hours (Kanamitsu et al. 2002).

Within the WRF framework, we applied a series of parameterizations to simulate cumulus, surface, radiative, and boundary layer processes. To simulate microphysics,

we used the WRF single-moment 6-class scheme, which includes parameterizations for ice, snow, and graupel and is suitable for high-resolution modeling experiments (Hong and Lim 2006). Longwave radiation was simulated with the Rapid Radiative Transfer Model and shortwave radiation used the Dudhia scheme. The surface layer used similarity functions with the fifth-generation Pennsylvania State University–National Center for Atmospheric Research Mesoscale Model (MM5) scheme, and the boundary layer was parameterized with a nonlocal K scheme and explicit entrainment. Finally, the Kain–Fritsch scheme was used for our cumulus parameterization (Skamarock et al. 2008).

The Noah land surface model includes four soil layers that are 10, 30, 60, and 100 cm thick, for a total of 2 m of simulated soil. The coupled model also has a canopy layer and, when applicable, a snow layer. Vegetation and soil parameters were set using the 20-category, 30-arc-s Moderate Resolution Imaging Spectroradiometer (MODIS) land use dataset (Friedl et al. 2002). Soil moisture was initialized from two-layer NCEP–DOE Reanalysis 2 moisture fields. This introduces some uncertainty in modeling changes due to deforestation as differences between surface vegetation could lead to changes in soil moisture storage (Hong et al. 2009). To calculate latent heat flux from different vegetation types, Noah calculated the sum of fluxes from ground and vegetation evaporation and transpiration, as well as sublimation from snowpack when applicable (Chen and Dudhia 2001; Hong et al. 2009). Precipitation can be intercepted and stored on the vegetative layer, but surface moisture that is not absorbed by the soil is lost as runoff. This lack of puddling may introduce small biases into the surface energy budget. These moisture fluxes were calculated through linear methods and depended on parameters based on the MODIS vegetation and soil type.

b. Determination of drought extent and magnitude

We used a combination of simulated volumetric soil moisture estimates and maximum climatological water deficit (MCWD; Aragão et al. 2007) as measures of historical and simulated drought extent and magnitude in the Amazon basin. Specifically, we estimated MCWD that occurred over the simulated time period (April–September) within the Amazon basin south of the equator. We chose 0° latitude as a cutoff for this calculation for two reasons. First, as shown in Fig. 1, the majority of deforestation is located in the arc of deforestation south of 0°, so we wanted to focus on drought in regions most likely to be impacted by land cover change. Second, north of 0° the seasonal pattern of precipitation changes such that April–September is no longer the dry season. As a result, the April–September precipitation increases, which tends to minimize MCWD north of 0° and cause spuriously extreme values when normalized because of low variance. This measure of drought intensity assumes a constant evapotranspiration (ET) rate of 100 mm month^{-1} over the tropical rain forest, which was based on in situ observations taken from various locations around the Amazon rain forest. Further, we assumed that when the rate of precipitation is below 100 mm month^{-1} for a given grid point, vegetation in that grid point begins to be stressed and is in a state of water deficit. If that state persists, the water deficit increases until the precipitation rate rises above 100 mm month^{-1}, at which point the water deficit diminishes. Following Aragão et al. (2007), we formally calculated the water deficit (WD) at a given grid point (i) at time t as

$$\mathrm{WD}_{t-1}(i) = \min[0, \mathrm{WD}_{t-1}(i) - E + P_t(i)], \qquad (1)$$

where E is the assumed rate of ET (=100 mm month^{-1}) and P (mm month^{-1}) is the rate of precipitation. The MCWD was the most negative value that the water deficit incurred over the April–September time period. The MCWD was then normalized across the simulation years. We calculated observed MCWD using satellite data from the Tropical Rainfall Measuring Mission (TRMM), which was designed to monitor and evaluate tropical rainfall magnitude and frequency (NASA 2006). This monthly mean data was available at 0.25° × 0.25° resolution from 1998–2011. It should be noted that it has been suggested that this dataset tends to underestimate extreme drought impacts in the Amazon (Aragão et al. 2007).

c. Land cover change datasets

To estimate the extent of land cover change and deforestation in the Amazon basin, we used 5-min spatial resolution data from Ramankutty et al. (2008) describing the composite fractional area of all croplands and pasturelands for the year 2007 and the potential vegetation dataset described in Ramankutty and Foley (1999) to determine the potential extent of the Amazon rain forest in the absence of anthropogenic influences. By comparing the potential extent of the rain forest to the observed cropland and pastureland, we estimated the fractional extent of tropical rain forest that had been converted to cropland and pasture (Fig. 1). Where the fractional extent of crop and pasture was found to have become the dominant (>0.5) land type, we forced the vegetative state of our model to be represented by pasture for the deforestation scenario. Where the fractional land use extent was greater than 0.05 but less than 0.5, the vegetation was converted to a crop–forest mix.

Finally, in the small number of regions at the rain forest's edge, where the model's default rain forest extent differed from the potential vegetation dataset, the land type was converted to tropical rain forest to maintain consistency. This process neglected the extensive small-scale changes and selective logging that are currently widespread in the Amazon basin, as these changes are not accounted for in the pasture and cropland data of Ramankutty et al. (2008) (Alves et al. 2009).

To test our coupled mesoscale model's surface flux and boundary layer responses to land cover change, we used flux and boundary layer height data from the Anglo-Brazilian Amazonian Climate Observations Study (ABRACOS) and Rondonia Boundary Layer Experiment (RBLE). Concurrent observations at two sites were taken in close proximity to test the impacts of land use change on surface fluxes and the atmospheric boundary layer. This first site was located at 10°5′S, 61°55′W in an undisturbed tropical forest surrounded by a 95% undisturbed forest. The second site was located at 10°45′S, 62°21′W on a cattle ranch (Fig. 1). During the RBLE, radiosondes were launched at standard times during intensive study periods throughout the 1991–94 dry seasons to observe changes in boundary layer conditions due to differences in land cover (Culf et al. 1996; Gash and Nobre 1997; Fisch et al. 2004; von Randow et al. 2004). To assess the ability of WRF-Noah to simulate changes in surface energy balance and boundary layer height associated with deforestation, the averages of these observations were compared to the mean simulated impacts from deforestation in the six study years described in section 2a.

d. Back-trajectory and recycling calculations

Using Lagrangian quasi-isentropic back-trajectory (QIBT) analysis described in Brubaker et al. (2001) and extended in Dirmeyer and Brubaker (2007), we identified the evaporative source (where moisture that precipitates out of the atmosphere last evaporated off Earth's surface) and precipitative sink (where moisture that evaporated from a given regions falls as precipitation). Comparing dry season spatial patterns of evaporative source and precipitative sink across model runs, we analyzed how the patterns changed under natural variability and deforestation. QIBT was performed on 10-min time steps of linearly interpolated hourly WRF output for the dry season of each model run. First, we calculated the total precipitation for every grid cell in our domain for the 18 pentads from 2 July to 30 September. Next, for each cell where precipitation occurred, 100 parcels were initialized at times when precipitation occurred throughout the pentad. As such, each parcel represented $^1/_{100}$ of the total pentad precipitation. The initial height and locations of these parcels within a grid cell "*i*" were quasi random, and each parcel was tracked backward in time and space along isentropic lines. As the parcel passed over a neighboring grid cell "*j*," a fraction of the precipitation represented by the parcel was attributed to ET at grid cell *j* equal to the ET of the grid cell divided by the total column precipitable water. Combined with other parcels that passed over grid cell *j*, this represented the evaporative source of grid cell *i* at grid cell *j* (Dirmeyer and Brubaker 2007; Harding and Snyder 2012). Iterating this process backward in time, the evaporative source was continually calculated for each grid cell the parcel passed over until all the precipitation was accounted for, 7 days had passed, or the parcel reached the edge of the domain. The evaporative source information stored within the parcel was then aggregated with the 99 other parcels for grid cell *i* to determine the pattern of where precipitation from grid cell *i* last evaporated off Earth's surface. Because the backward trajectories link precipitation over one grid cell to ET in other grid cells upstream, this technique can also be used to create forward trajectories, yielding the precipitation field that results from ET over each grid cell. The major assumption in this process was that ET of a given grid cell was well mixed throughout the air column.

By aggregating the QIBT analysis over a given time period and region, we calculated precipitation recycling ratios (R), which are defined as the fraction of rainfall over a given region that last evaporated from the region itself. We calculated this measure for a subregion of our domain (green box in Fig. 1). To calculate the recycling ratio, we began by summing the evaporative source pattern for all the grid cells within our subregion. Next, the evaporative source that originated outside the subregion itself was removed. The remaining evaporative source represented the precipitation of recycled origin (P_{rec}). Finally, we divided this by the total precipitation of the subregion (P_{tot}) to find the recycling ratio:

$$R = \frac{P_{\text{rec}}}{P_{\text{tot}}}. \tag{2}$$

Recycling ratios are important measures of the magnitude of land–atmosphere coupling in the atmospheric branch of the hydrological cycle for a given region (Brubaker et al. 1993; Dirmeyer et al. 2009; van der Ent et al. 2010; Bagley et al. 2012). A major advantage of using QIBT to determine recycling ratios over analytical methods is that it removes the reliance on time-averaged hydrological variables that may not be representative of short-duration precipitation events (Brubaker et al. 2001).

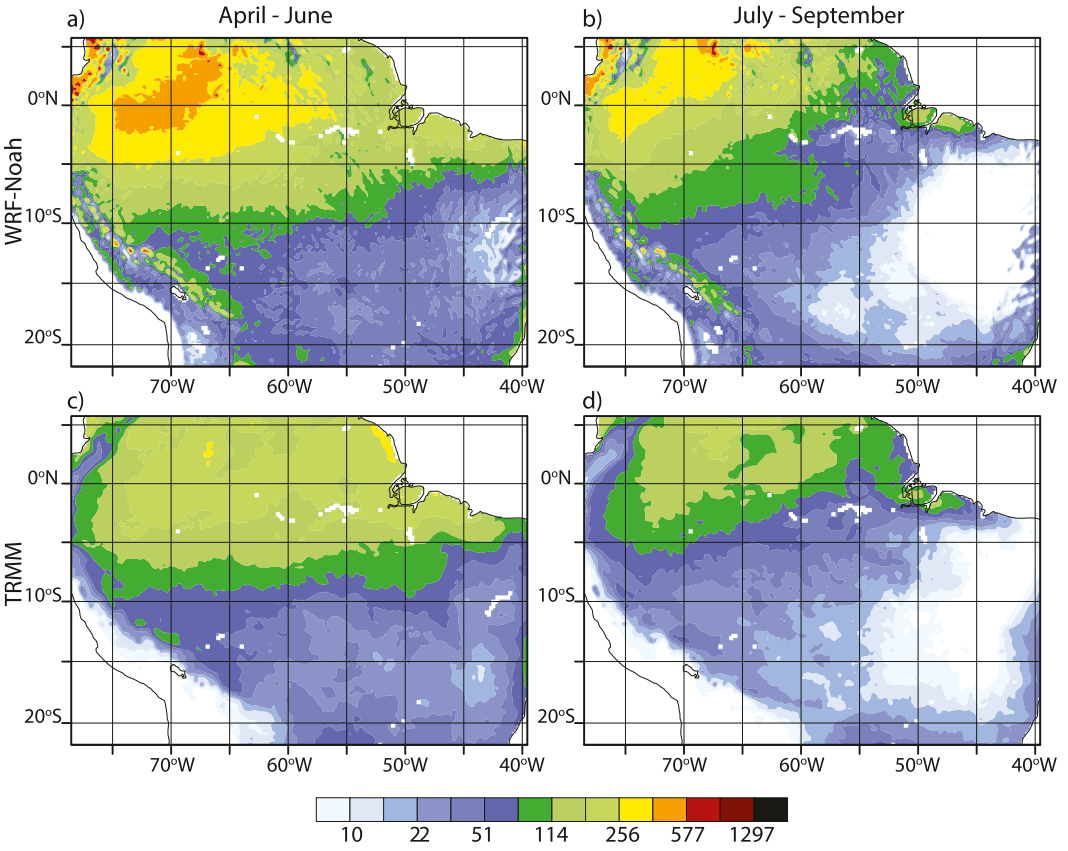

FIG. 2. Mean precipitation rates (mm month^{-1}) from (a),(c) AMJ and (b),(d) JAS from the potential vegetation (top) WRF-Noah simulations and (bottom) TRMM observed precipitation data. Note that each increment in the scale is 1.5 times the previous value.

3. Results

a. Observed and simulated precipitation regimes

To validate that WRF-Noah was reproducing the observed drought variability and mean rainfall over our domain for the April–September simulation period, we compared the precipitation fields for the natural vegetation runs averaged across the six simulation years to mean TRMM fields across the same time period (Fig. 2). We found that WRF-Noah was able to reproduce the change in precipitation patterns that occurs between the austral fall months of April–June (AMJ) months and the JAS dry season months. In the northern part of the domain, WRF-Noah overestimated precipitation for both the AMJ and JAS seasons relative to the TRMM precipitation fields. In the southern portion of the Amazon basin (<5°S) WRF-Noah precipitation fields better matched observed values. However, positive biases were still evident, particularly in the wetter western portion of the domain. WRF-Noah also reproduced the large latitudinal gradient in precipitation that occurred within our simulation domain, with typical northern precipitation rates reaching values two orders of magnitude larger than typical values found in the southern portion. Finally, WRF-Noah appeared to overestimate topographical precipitation in the Andes.

Over the simulated dry seasons, the areal mean precipitation rates and the areal mean standardized volumetric soil moisture (SVSM) for the WRF-Noah natural vegetation scenarios clearly differentiated the pluvial, normal, and drought years (Table 1). As has been shown by previous studies, the precipitation anomalies during these years were unique in that they were largely driven by sea surface temperature in the North Atlantic, with strongly positive AMO indices being indicative of drought conditions in the Amazon and ENSO playing a secondary role, unlike previous droughts in the region (Marengo et al. 2011).

Comparing the spatial patterns of MCWD from TRMM for our selected drought years of 2005 and 2010 revealed large differences in the drought epicenters and magnitudes (Figs. 3i,l). Similar to the results shown in Lewis et al. (2011), the observed drought epicenter in 2005 was located in the southwest Amazon basin. This

TABLE 1. Areal mean SVSM calculated from July to September for WRF-Noah potential vegetation simulations for the southern Amazon basin. Also shown are WRF-Noah simulated mean precipitation rates (mm month^{-1}) for April–September for the southern Amazon basin and the sign of the AMO and ENSO using Kaplan SST, version 2.

Year	2003	2004	2005	2007	2009	2010
WRF-Noah SVSM	−0.04	0.51	−0.65	0.32	0.58	−0.69
WRF-Noah precipitation rate	236.4	257.8	215.7	237.55	245.4	223.5
ENSO state	Neutral	Positive	Neutral	Slightly negative	Transition negative to positive	Transition positive to negative
AMO state	Slightly positive	Slightly positive	Very positive	Neutral	Negative	Very positive

drought was limited in spatial extent, with much of the eastern and northern domain experiencing normal or wet conditions. The year 2010 was the more severe drought year, with three major drought epicenters located in the western, southern, and southeastern Amazon basin. These patterns of drought were reproduced in our WRF-Noah simulations (Figs. 3c,f), although the epicenter of the 2005 simulated drought was to the northwest of that observed using TRMM. For 2009 both observed and simulated MCWD (Figs. 3e,k) exhibited wet conditions across the southern Amazon, with simulated MCWD slightly more localized and intense in the eastern Amazon relative to observations. Finally, observed MCWD in 2003 and 2007 (Figs. 3h,k) did not exhibit any extreme conditions, with slightly dry conditions persisting in 2007 and slightly wet conditions across the domain in 2003. The WRF-Noah simulations for these years similarly did not produce any extremes (Figs. 3a,d). However, the simulations developed slightly drier than observed conditions in 2003 and wetter than observed conditions in 2007.

Finally, we tested the model's ability to reproduce surface and boundary layer impacts of land use change using the flux and radiosonde data from the paired pasture/rain forest site in the southern Amazon basin described in section 2c (starred location in Fig. 1). Using the subset of simulation grid points that were converted to pasture in our land use change simulations (i.e., fractional land use >0.5), we selected the point closest to the observational site. Then, using the average of the 2003, 2004, 2005, 2007, 2009, and 2010 dry season model simulations for this point, the changes in surface energy fluxes and boundary layer height with land cover change were compared to the average observed impacts of deforestation from the paired pasture/rain forest site. We found the model reproduced the key shifts in the surface energy balance and boundary layer height with deforestation. At the paired site deforestation caused the observed midday net radiation to decrease by 102 W m^{-2}, sensible heat flux to increase by 65 W m^{-2}, latent heat flux to decrease by 179 W m^{-2}, and maximum boundary layer height to increase by ~570 m. Similarly, at our simulated point, the mean midday net radiation decreased by 56 W m^{-2}, sensible heat flux increased by 32 W m^{-2}, latent heat flux decreased by 95 W m^{-2}, and the maximum boundary layer height increased by ~70 m. Combined

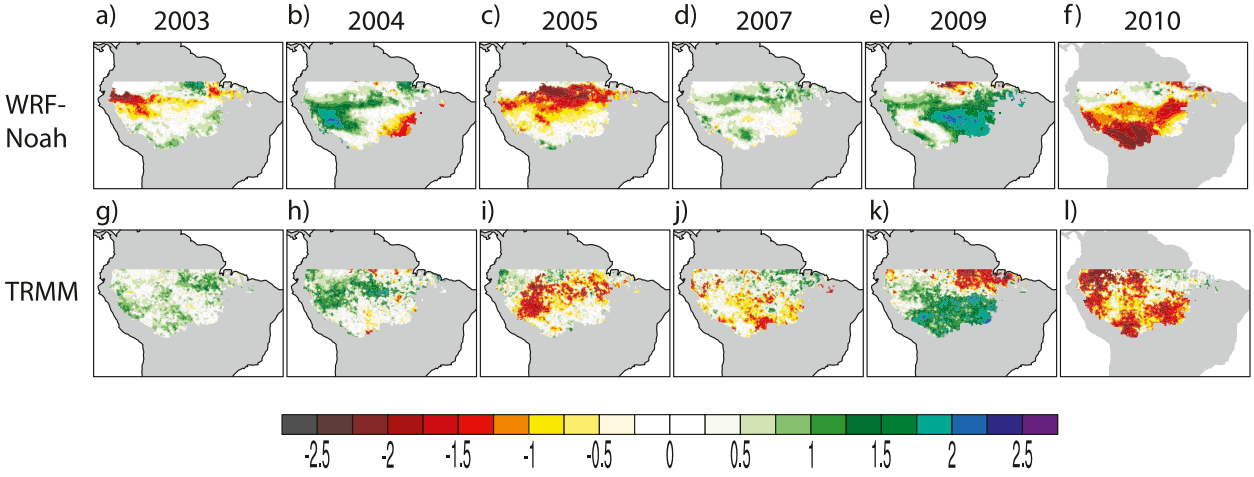

FIG. 3. Normalized MCWD calculated for April–September from WRF-Noah potential simulations including (top) deforestation and (bottom) TRMM observations for (a),(g) 2003; (b),(h) 2004; (c),(i) 2005; (d),(j) 2007; (e),(k) 2009; and (f),(l) 2010.

TABLE 2. Simulated mean difference of surface and meteorological variables due to deforestation for April–June and July–September across all simulation years. Areal averages are taken over the entire Amazon rain forest region (columns 2 and 3), and only those points are converted to pasture (columns 3 and 4). The percent changes are shown in parentheses.

	Full Amazon rain forest region		Region converted to pasture	
	April–June	July–September	April–June	July–September
Precipitation rate (mm month^{-1})	−9.36 (−3.16%)	−9.47 (−5.45%)	−32.51 (−16.27%)	−25.72 (−18.53%)
Sensible heat flux (W m^{-2})	−0.758 (−2.75%)	1.04 (+2.30%)	−0.14 (−0.65%)	6.26 (+11.44%)
ET (mm month^{-1})	−2.68 (−1.94%)	−5.95 (−4.61%)	−15.89 (−13.42%)	−28.37 (−29.55%)
Net surface radiation (W m^{-2})	−4.39 (−2.45%)	−4.82 (−2.50%)	−4.02 (−2.48%)	−10.11 (−6.04%)
Boundary layer height (m)	−6.21 (−1.27%)	3.90 (+.62%)	−5.95 (−1.28%)	28.29 (+4.25%)
2-m temperature (K)	−0.10	+0.036	−0.033	+0.32
2-m specific humidity (kg kg^{-1})	−5.74E-5 (−0.41%)	−1.50E-4 (−1.04%)	−1.84E-4 (−1.30%)	−4.67E-4 (−4.10%)
Lifting condensation level (m)	−4.49 (−0.56%)	31.31 (+2.31%)	7.08 (+.58%)	105.38 (+5.66%)

with WRF-Noah's reproduction of the precipitation and drought patterns, this information gives confidence to the ability of WRF-Noah to simulate the impacts of deforestation under varied rainfall regimes.

b. *Impact of land use change on mean surface fluxes and meteorological variables*

The larger impacts from land cover change across all April–September simulations occurred during JAS relative to AMJ (Table 2). Land cover change reduced precipitation by 5.45% and ET by 4.61% over the entire rain forest region during the dry season, but only 3.16% and 1.94% during AMJ. Additionally, over the grid points that had been converted to pasture, the difference in ET was larger, with reductions of nearly 30% during the JAS dry season but only 13.4% in AMJ. Along with changes in net radiation and sensible heat flux, the changes in ET forced alterations to the boundary layer state and atmospheric stability. Over regions converted to pasture, altered surface energy fluxes that resulted in a dry season increased near-surface temperature (+0.32°C) from increased sensible heating (+11.44%), increased lifting condensation level (+5.66%), and decreased near-surface specific humidity (−4.10%).

The atmospheric and hydrological impacts of tropical deforestation were not locally constrained to the immediate regions of land cover change, but rather, were spread across the region by the atmospheric circulation (Fig. 4a). For the most part, changes in atmospheric circulation from land cover change were small (Fig. 4b) relative to changes in drought versus pluvial years (Fig. 4c). However, there was some evidence of increased low-level convergence due to land cover change over the epicenters of deforestation in the southern Amazon and divergent flow near the Pará and Maranhão states of northeast Brazil. The changes from deforestation (Fig. 5) in temperature at the lowest atmospheric model layer (Fig. 5f) appeared to be largely constrained to the large regions of land cover change in the southern Amazon. However, the response of precipitable water (Fig. 5e) and precipitation (Fig. 5d) to deforestation were more diffusely spread across the domain. In the precipitation field, there was evidence of drying along the southern arc of deforestation and of strong drying in the northwest corner of the domain. The remainder of the northern portion of the domain appeared to experience an increase in rainfall. The pattern of change for precipitable water was more coherent. Along the arc of deforestation, precipitable water dropped because of reduced moisture fluxes from the surface, and this reduction was advected to the south and northwest by prevailing wind patterns and the northerly low-level jet, which are strongly linked to the South American convergence zone (Nobre et al. 2009).

c. *Variation of land cover change impacts under drought and pluvial conditions*

In the 850-mb circulation patterns and moisture flux, we found that drought years were characterized by reduced northeasterly onshore flow from the tropical Atlantic Ocean in northeast Brazil (Fig. 4c). This pattern extended south into the northern portion of the Amazon basin. This reduced moisture availability for precipitation in recent drought years.

When we compared the impacts of land cover change (Table 2) with the mean impacts of the precipitation regimes, we found that the natural variation of rainfall between drought and pluvial years dominated changes over the entire region. However, on local scales, changes from land use during the dry season were of the same magnitude or larger than those from changes in precipitation regimes. However, in the natural environment, changes from climatological rainfall variability and deforestation do not act independently of each other. Instead, changes in moisture, energy, and momentum from deforestation feedback alter the patterns and magnitudes

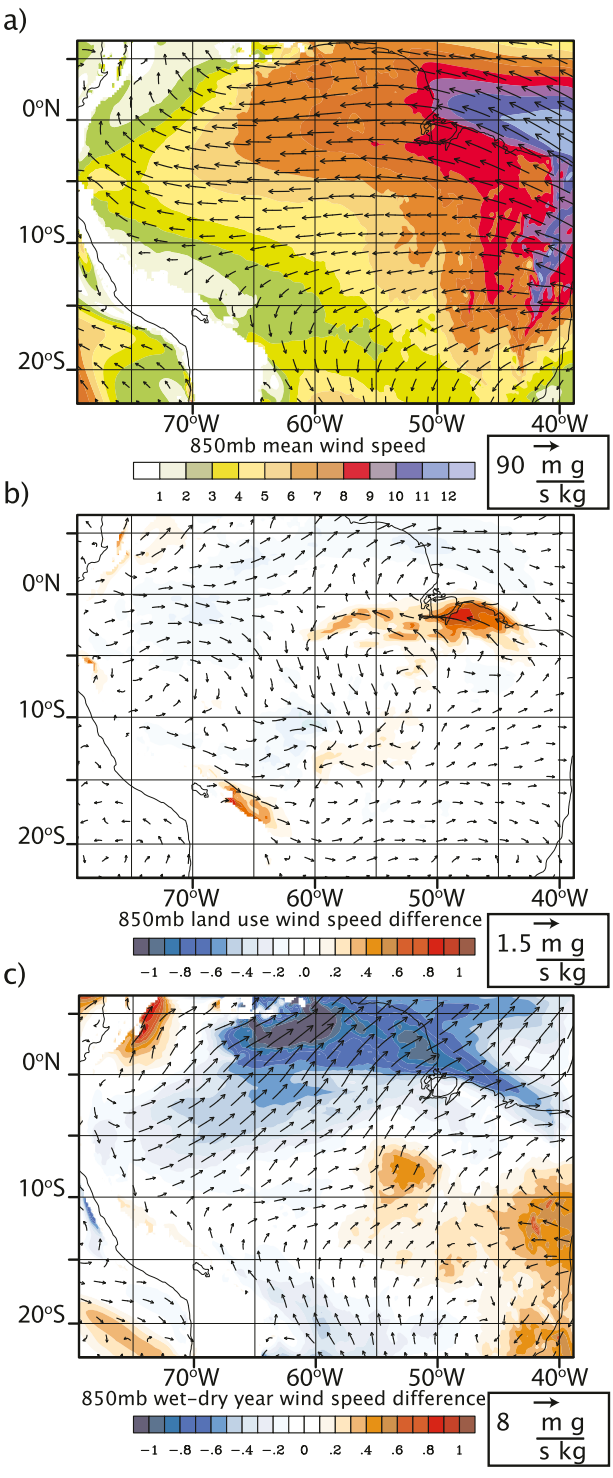

FIG. 4. (a) The JAS WRF-Noah simulated mean 850-mb moisture flux ($m\,s^{-1}\,g\,kg^{-1}$) (arrows) and mean 850-mb wind speed ($m\,s^{-1}$) (shaded) averaged across all potential vegetation simulations. (b) The simulated change in moisture flux and wind speed with deforestation at 850 mb averaged across all simulation years. (c) The difference between mean drought and pluvial year moisture flux and wind speed at 850 mb from potential vegetation simulations.

of precipitation associated with natural variability, and it can be expected that a deforested region will respond differently to drought conditions versus pluvial conditions.

The impacts of deforestation on precipitation, precipitable water, and low-level temperature (Figs. 5d–f) were most extreme in the south-central and northwest Amazon. This is the same location where precipitation and precipitable water were strongly perturbed during drought conditions. However, in the northwest Amazon the rates of precipitation were extremely high during JAS as a result of the northern position of the intertropical convergence zone (Fig. 2). As a result, the fractional impact of deforestation in the northwest Amazon during JAS was very small. This indicates potential positive feedbacks between drought and land cover change in the southern Amazon near the arc of deforestation. During the JAS dry season, we found the impacts of land cover change over Amazon basin were most extensive during the drought years relative to the pluvial and normal years (Table 3). In the immediate regions of land cover change, the differences between deforestation impacts during pluvial and drought years were larger.

In regions of land cover change, deforestation resulted in a decrease of JAS mean precipitation of 17.08% during pluvial years and 20.15% during drought years. Similarly, during pluvial years, deforestation led to an increase of sensible heat flux of 9.4% and an increase of 13.76% during drought years across regions of deforestation. Finally, deforestation locally caused mean latent heat flux to decrease by 25.70% during pluvial years and 32.84% during drought years. During AMJ, the differences in impacts due to deforestation were minimal between drought, normal, and pluvial years (not shown).

Finally, averaging the volumetric soil moisture over the tropical rain forest south of the equator and using it as a proxy for drought magnitude, we found that land cover change reduced mean volumetric soil moisture in all years (Table 4). During pluvial years, the wet conditions were decreased with land cover change and drought conditions were increased. The mean change from deforestation during the pluvial years of 2004 and 2009 was a reduction in mean volumetric soil moisture of 3.00%. During the 2003 and 2007 normal years, it was reduced by 3.86%, and during the 2005 and 2010 drought years, the mean change was a reduction of 4.38%. These results suggest that land cover change has likely contributed to the intensity of recent drought events and that the impact of land cover change was amplified during drought conditions in the southern Amazon.

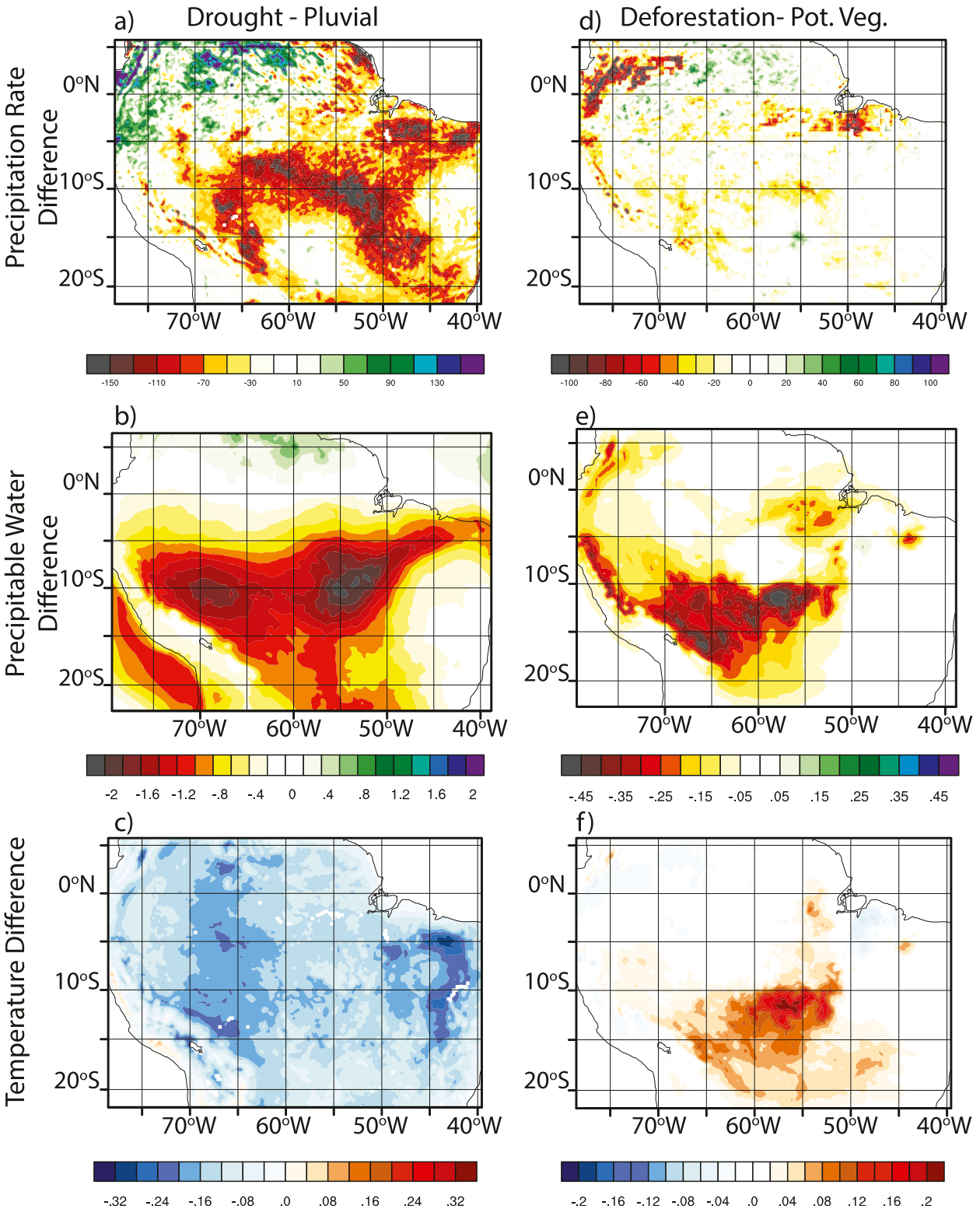

FIG. 5. (left) Mean dry season difference in drought year relative to pluvial year and (right) mean changes from deforestation across all simulation years of (a),(d) precipitation rate (mm month^{-1}); (b),(e) precipitable water (mm); and (c),(f) temperature of the bottom atmospheric model level (K).

TABLE 3. Simulated areal mean changes in surface and meteorological variables from deforestation for July–September during drought and pluvial years. Averages are taken over the entire Amazon rain forest region.

	July–September		
	Pluvial years	Normal years	Drought years
Δ Precipitation rate	−4.99%	−5.58%	−5.93%
Δ Sensible heat flux	+.48%	+3.12%	+4.28%
Δ ET	−3.63%	−4.65%	−5.57%
Δ Net surface radiation	−2.41%	−2.48%	−2.70%
Δ Boundary layer height	−0.11%	+.86%	+1.36%
Δ 2-m specific humidity	−0.77%	−3.21%	−1.31%
Δ Lifting condensation level	+1.29%	+3.36%	+3.94%

d. Back-trajectory analysis of moisture from altered land cover and moisture recycling over the Amazon basin

Figure 6 shows where the water that evapotranspired from grid points with observed land use fractions greater than 0.05 fell as precipitation across the potential vegetation simulations. The sum of forward trajectories for land use change points within our domain indicates that nearly all of the moisture that evapotranspires from points of deforestation within this region precipitated over land, with the Andes acting as a barrier to moisture flow (Fig. 6a). Additionally, while the most extreme amounts of moisture precipitated in the northwest corner of the domain, relatively large amounts of terrestrial evaporation from deforested regions did return to the surface in the central and southern Amazon. A comparison of Fig. 6 and Fig. 2 suggests that in parts of the southern Amazon, this terrestrial contribution represented more than half of the total simulated dry season precipitation. Breaking the forward trajectories into subcategories, we found where moisture from land use points within the recycling region (RR), northwest land use region (NW), south-central land use region (SC), and eastern land use region (E) as defined in Figs. 6b–e precipitated out of the atmosphere. While the majority of the moisture from the NW region was locally recycled, relatively large portions of the water vapor from the SC and E regions were advected out of their respective domains.

Differences in forward trajectory precipitation between drought and pluvial years for the potential vegetation simulations (Fig. 7) revealed that during drought years, less moisture from regions of land cover change rained out over the central Amazon and more precipitated in the northern portion of our domain. Several factors contributed to this. First, points of land cover change in the northern portion of the domain experienced increased precipitation during drought years, as shown in Fig. 5. This generally increased latent heat flux over these points, increasing their contribution to the northern precipitation events that had back trajectories passing over them. Also, changes in circulation played a role in increasing forward trajectory precipitation in the northern portion of the domain and reducing it elsewhere. This was evident in Fig. 7d, where forward trajectories from the E region were reduced directly westward of the region of deforestation but increased to the north.

While changes in forward trajectory precipitation with deforestation were smaller in magnitude compared to changes from rainfall regimes, they had a negative precipitation impact over the entire domain, with the exception of the southeast portion where changes were negligible (Fig. 8). This deforestation-induced precipitation reduction occurred over nearly the entire central and western portion of domain east of the Andes. Deforestation-induced precipitation reduction was also evident throughout the southern Amazon basin drought regions, as shown in Fig. 8a. Much of this reduction was due to deforestation in the SC region (Fig. 8e), with small contributions from deforestation in the EA region (Fig. 8d). Deforestation in the NW region did not reduce precipitation in the drought region (Fig. 8c).

Using QIBT analysis, we collected the total recycled precipitation and total precipitation over the recycling region (green box in Fig. 1) and calculated the recycling ratio for JAS during drought and pluvial years using Eq. (2). We found that the percentage of recycled water in our recycling domain increased from 66.6% in JAS during pluvial years to 73.9% in drought years. Extracting the recycling data from August (the month most strongly impacted by drought conditions) results in precipitation recycling increasing from 70.9% in pluvial

TABLE 4. Areal mean volumetric soil moisture ($m^3 m^{-3}$) for July–September for natural vegetation and deforestation scenarios. Also shown is the percent change in volumetric soil moisture due to deforestation averaged over pluvial, normal, and drought years.

Year	2003	2004	2005	2007	2009	2010
Mean soil moisture natural vegetation scenario ($m^3 m^{-3}$)	0.303	0.307	0.294	0.305	0.320	0.286
Mean soil moisture deforestation scenario ($m^3 m^{-3}$)	0.290	0.297	0.282	0.294	0.311	0.273
Mean pluvial year difference		Mean normal year difference			Mean drought year difference	
−3.00%		−3.86%			−4.38%	

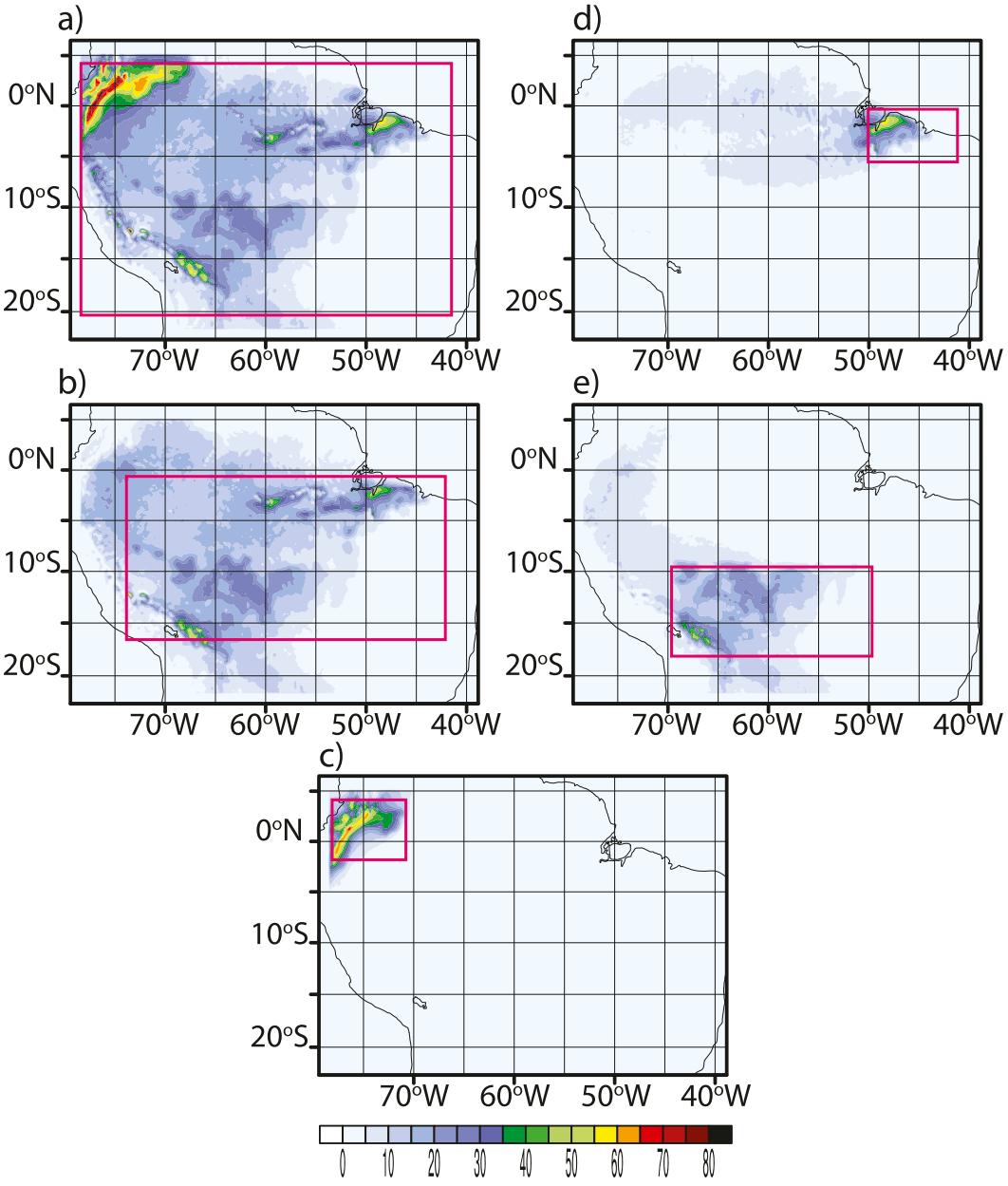

FIG. 6. Dry season simulated mean forward trajectory precipitation (mm month^{-1}) from grid points with land cover change greater than 0.05 in Fig. 1. Forward trajectory precipitation fields are shown for land cover change points in the majority of (a) the domain, (b) the recycling region, (c) the NW region, (d) the E region, and (e) the SC region (pink boxes). These trajectories represent the potential vegetation simulations and are averaged over all simulation years.

years to 83.3% during drought years. During the normal simulated years, the percentage of recycled precipitation was between the pluvial and drought values, with 67.3% during JAS and 75.0% during August alone. These increases in precipitation recycling were likely a direct result of reduced onshore moisture flow from the Atlantic Ocean (Fig. 4). With reduced moisture from the Atlantic Ocean more precipitation was the result of convection condensing water that had been locally evaporated from the land surface. This indicated increased reliance on local moisture sources for precipitation during drought years and supported our hypothesis that the impacts of land cover change were increased during recent drought conditions in the Amazon basin. The change in recycling ratio with deforestation was small in these simulations, with uniform increases in recycling

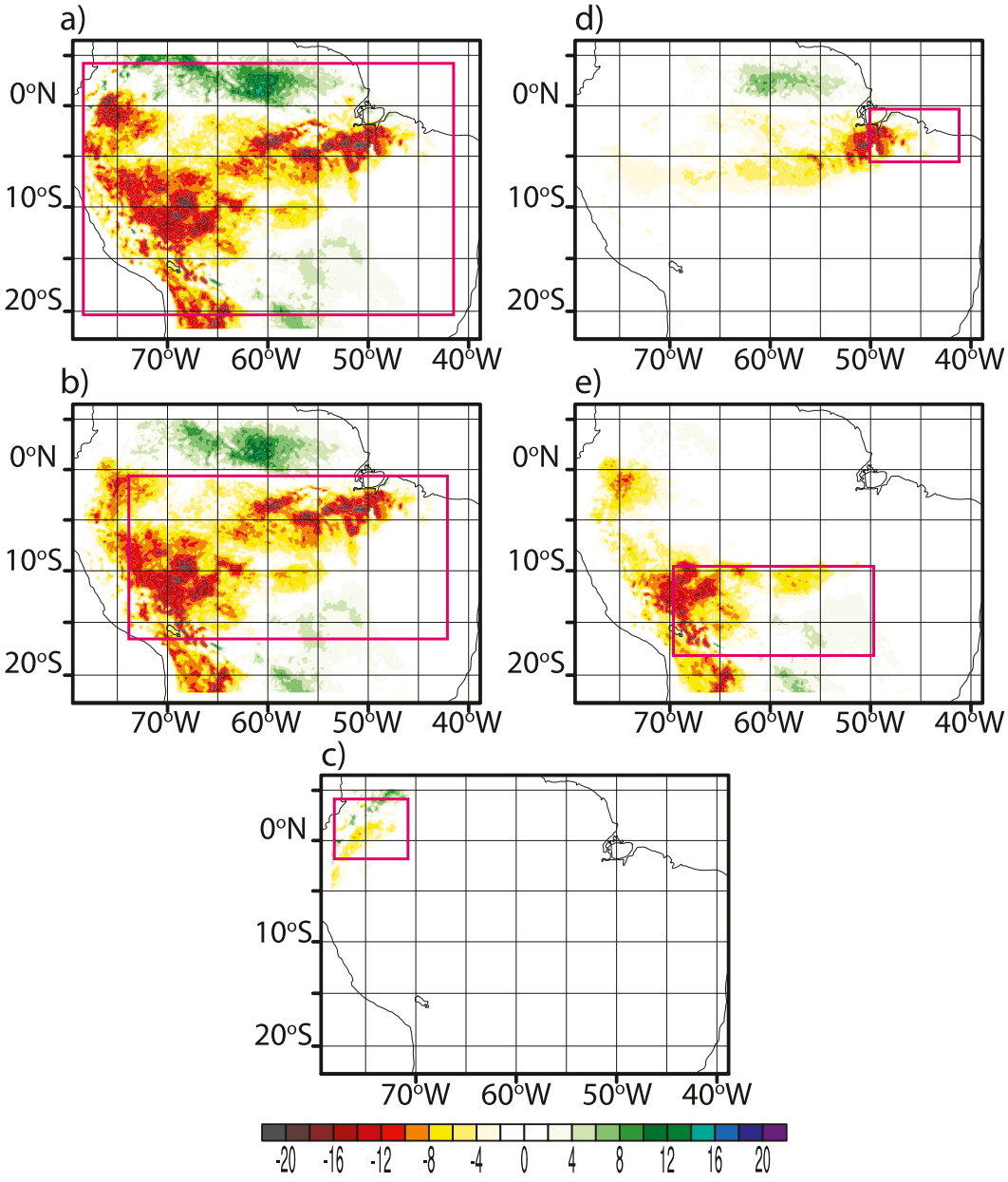

FIG. 7. Dry season simulated mean difference between drought and pluvial forward trajectory precipitation (mm month^{-1}) from grid points with land cover change greater than 0.05 in Fig. 1. Forward trajectory precipitation anomalies are shown for land cover change points in the majority of (a) the domain, (b) the recycling region, (c) the NW region, (d) the E region, and (e) the SC region (pink boxes). These trajectories represent the potential vegetation simulations.

with deforestation of ~1%. This again suggested that deforestation did not have extensive influence on circulation patterns in the region for our simulations. Instead, the primary effect was a decrease in precipitable water due to changes in surface latent heat fluxes. This decrease in precipitable water led to less moisture being available for precipitation at the deforested area's precipitative sink but did not notably change its location.

4. Discussion

This study focused on the impacts of land cover change and precipitation variability over the Amazon basin. In particular, we tested how the impacts of deforestation changed under recent varied rainfall regimes. Drawing from our analysis, there were several results that should be highlighted. First, while

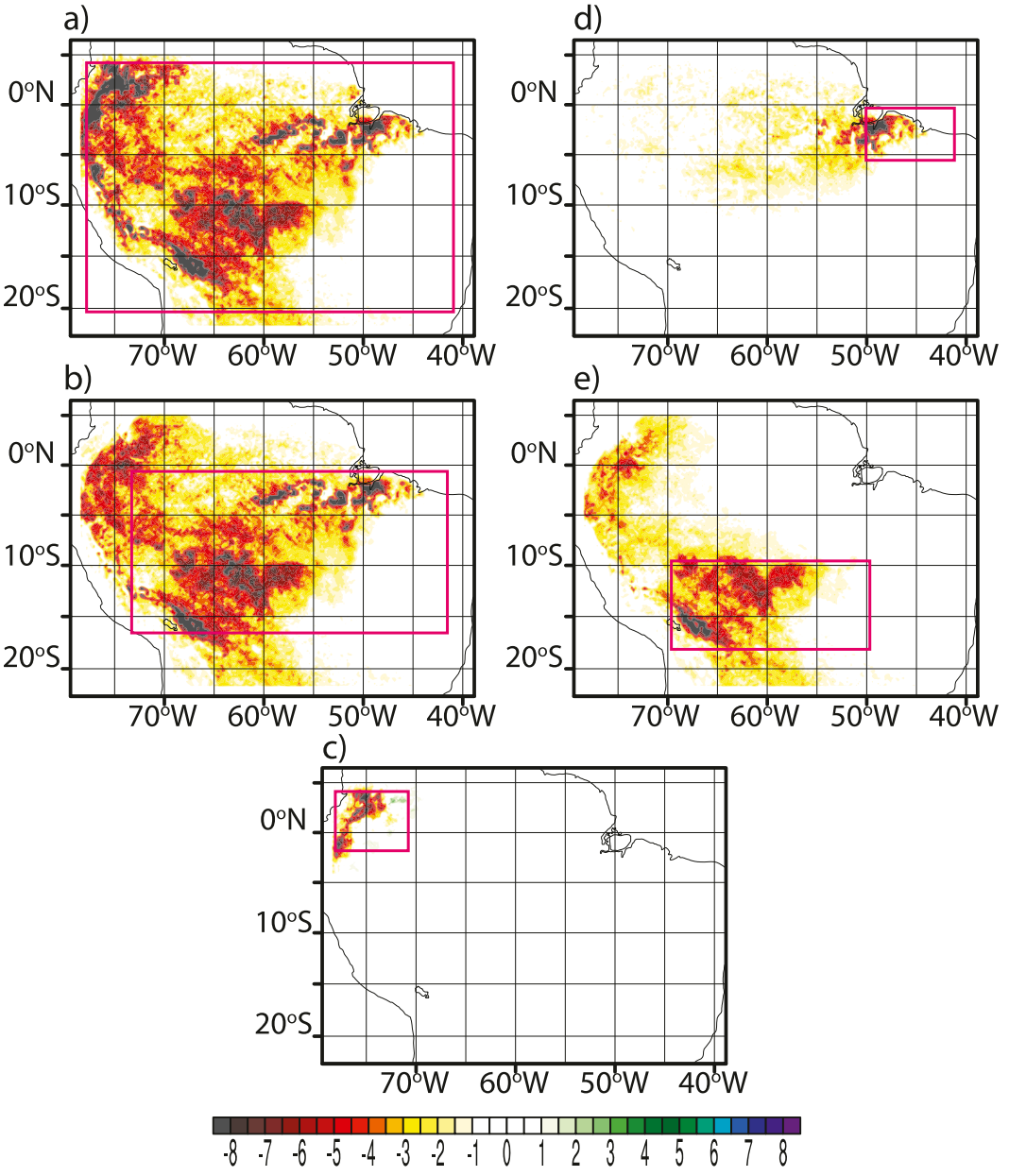

FIG. 8. Dry season simulated impact of deforestation on forward trajectory precipitation (mm month^{-1}) from grid points with land cover change greater than 0.05 in Fig. 1. Forward trajectory precipitation changes from deforestation are shown for land cover change points in the majority of (a) the domain, (b) the recycling region, (c) the NW region, (d) the E region, and (e) the SC region (pink boxes). These trajectories are averaged over all simulation years.

large amounts of dry season moisture evapotranspired from regions of deforestation were locally recycled, portions were advected and fell as precipitation to the south and in the center of the Amazon basin. Second, while we did not find evidence of extensive shifted spatial patterns of precipitation, deforestation reduced the magnitude of precipitation in the regions mentioned above. Also, during drought years the percentage of precipitation that was locally recycled increased by 12.4% during August and 7.3% over the entire dry season. This was partially due to reduced advection of Atlantic moisture into the recycling region. Finally, we found current levels of deforestation have the potential to enhance the magnitude of severe drought. Coupled with increased precipitation recycling in drought years, this represents a positive feedback to reductions in precipitation associated with natural variability.

The impact of deforestation on recent drought may have implications for the potential of climate to influence biomass in the Amazon rain forest. While recent work has suggested that the likelihood of climate-induced large-scale dieback of the tropical rain forest is low (Huntingford et al. 2013), there remains significant concern on the impact of drought on short-term biomass in the Amazon (Phillips et al. 2009; Lewis et al. 2011; Toomey et al. 2011). One aspect that has been shown to be an important contributor to future drought conditions is the potential for an increased prevalence of anomalously warm sea surface temperatures in the North Atlantic similar to that which has been shown to have a causal relationship to the 2005 and 2010 droughts (Phillips et al. 2009). The tools used in this study are not directly suitable for testing the impacts of deforestation and drought on changing rain forest biomass because of static vegetation and soil layers not reaching the extensive depths that have been observed in rain forest rooting profiles (Nepstad et al. 1994). Additionally, this rooting limitation may be responsible for some underestimation of contrast between the natural vegetation and deforestation scenarios. However, we have shown that moisture recycling is increased and deforestation has an increased influence on regional climate when conditions like the 2005 and 2010 droughts exist. This suggests realistic scenarios of land use change should be included in simulations of climate impacts on biomass in the Amazon rain forest.

The results of this work were found to be broadly consistent with other multiyear seasonal mesoscale studies of Walker et al. (2009) and Medvigy et al. (2011). While these studies had different goals and methodology, in each study the largest impacts of deforestation on regional hydrology were found in the dry season, and the overall impact of deforestation was a reduction of precipitation. The impacts on precipitation were generally less than those found in modeling studies using lower-spatial-resolution general circulation models (D'Almeida et al. 2007; Lee et al. 2011). However, while Medvigy et al. (2011) also found strong reductions in dry season precipitation in the northwestern Amazon, in the southeast Amazon they found increases in precipitation due to circulation changes in a region where very little changed in our study. There are several potential explanations for this difference, including differences in model physics and resolution, as well as our absence of land cover change outside the tropical rain forest region. Additionally, more work could be done using a fully coupled climate model to fully assess the statistical significance of these results.

This study represents one of the few high-resolution seasonal studies of the Amazon region, but the relatively small number of drought, normal, and pluvial years analyzed inhibits valuable statistical tests. While this is partially due to the computational costs associated with increasing the number of years analyzed, more fundamentally, the droughts of 2005 and 2010 represent unique conditions that were thought of as once-in-a-century-level events and are not easily replicated using historical boundary conditions. However, as discussed above, the conditions that gave rise to the 2005 and 2010 droughts may be a harbinger of more common conditions in the near future. While simulations of future conditions are beyond this scope of this study and may introduce additional uncertainty, such simulations could allow for more realizations of extreme drought conditions that can be analyzed more precisely for statistical significance.

Additionally, our modeling approach was limited by its reliance on reanalysis boundary conditions and specified sea surface temperatures, parameters that could change depending on the scale of land cover change. The set boundary conditions limit the capability of the model to simulate changes in circulation and fluxes of moisture and energy near the edges of the domain. We mitigated this somewhat by not using grid points within 100 km of the domain edge. Also, this study was restricted to the April–September time frame, and the results might be different if taken over the full October–September hydrological year. It would be interesting to similarly test the impacts of deforestation on the wet season. We would expect reduced impacts from deforestation during that season because of smaller differences in surface fluxes between pasture and rain forest. However, changes in surface friction and soil moisture would still persist, which could have regional influences on circulation and precipitation. Finally, we did not test how land cover change could influence seasonality, particularly the timing of the beginning and end of the dry season, which has been identified as being important for fully quantifying drought impacts.

5. Conclusions

Mesoscale model results for pluvial, normal, and drought years over the first decade of the twenty-first century suggest that variations associated with anomalous Atlantic sea surface temperatures were the dominant drivers of change in the Amazon basin. While the degree to which anomalous Atlantic sea surface temperature may be anthropogenically influenced is an openly debated subject, it is clear the direct human impact of deforestation has had an equal or greater impact for areas where extensive land cover change occurred. Our model analysis suggests a positive feedback between drought and land use for the Amazon basin. Our

results also reinforced the notion that the impact of deforestation is not limited to points of land cover change but advected across the region by regional circulation patterns. Much of the moisture evapotranspired by regions of deforestation fell as precipitation over the central and southern Amazon basin, which corresponded to the regions of major drought in 2005 and 2010, indicating potential feedbacks between deforestation and drought conditions. Finally, during drought years, the dry season recycling ratio increased by ~7% relative to pluvial years, while moisture fluxes from oceanic sources decreased. These results indicate that land–atmosphere coupling of the hydrological cycle increased during droughts in the region.

The results of this study suggest that land cover change has the potential to increase the impact of droughts in Amazon basin. This could have important consequences spanning multiple disciplines including, but not limited to, increased fire potential, reduced flow in the Amazon River and its tributaries, crop yields, and the reduction of carbon uptake by vegetation, all of which have been shown to accompany reduced precipitation in the region. Further testing and refinement of the conceptual framework is essential to reducing uncertainty of the impact of land use and drought on Amazon ecosystem services.

Acknowledgments. The authors are indebted to two anonymous reviewers for their comprehensive and constructive comments on this manuscript. This work was carried out in part using computing resources at the University of Minnesota Supercomputing Institute. We thank the NOAA/ESRL Physical Science Division for providing climatological reanalysis at www.esrl.noaa.gov/psd/. This work was accomplished through financial support from the National Science Foundation.

REFERENCES

Alves, D. S., D. C. Morton, M. Batistella, D. A. Roberts, and C. Souza Jr., 2009: The changing rates and patterns of deforestation and land use in Brazilian Amazonia. *Amazonia and Global Change, Geophys. Monogr.,* Vol. 186, Amer. Geophys. Union, 11–23.

Aragão, L. E. O. C., Y. Malhi, R. M. Roman-Cuesta, S. Saatchi, L. O. Anderson, and Y. E. Shimabukuro, 2007: Spatial patterns and fire response of recent Amazonian droughts. *Geophys. Res. Lett.,* **34,** L07701, doi:10.1029/2006GL028946.

Bagley, J. E., A. R. Desai, P. C. West, and J. A. Foley, 2011: A simple, minimal parameter model for predicting the influence of changing land cover on the land–atmosphere system. *Earth Interact.,* **15,** doi:10.1175/2011EI394.1.

——, ——, P. A. Dirmeyer, and J. A. Foley, 2012: Effects of land cover change on moisture availability and potential crop yield in the world's breadbaskets. *Environ. Res. Lett.,* **7,** 014009, doi:10.1088/1748-9326/7/1/014009.

Baidya Roy, S., and R. Avissar, 2002: Impact of land use/land cover change on regional hydrometeorology in Amazonia. *J. Geophys. Res.,* **107,** 8037, doi:10.1029/2000JD000266.

Brando, P. M., S. J. Goetz, A. Baccini, D. C. Nepstad, P. S. A. Beck, and M. C. Christman, 2010: Seasonal and interannual variability of climate and vegetation indices across the Amazon. *Proc. Natl. Acad. Sci. USA,* **107,** 14 685–14 690.

Brubaker, K. L., D. Entekhabi, and P. S. Eagleson, 1993: Estimation of continental precipitation recycling. *J. Climate,* **6,** 1077–1089.

——, P. A. Dirmeyer, A. Sudradjat, B. S. Levy, and F. Bernal, 2001: A 36-yr climatological description of the evaporative sources of warm-season precipitation in the Mississippi River basin. *J. Hydrometeor.,* **2,** 537–557.

Chen, F., and J. Dudhia, 2001: Coupling an advanced land surface–hydrology model with the Penn State–NCAR MM5 modeling system. Part I: Model implementation and sensitivity. *Mon. Wea. Rev.,* **129,** 569–585.

Coe, M. T., E. M. Latrubesse, M. E. Ferreira, and M. L. Amsler, 2011: The effects of deforestation and climate variability on the streamflow of the Araguaia River, Brazil. *Biogeochemistry,* **105,** 119–131.

Costa, M. H., and J. A. Cardille, 2003: Effects of large-scale changes in land cover on the discharge of the Tocantins River, southeastern Amazonia. *J. Hydrol.,* **283,** 206–217.

——, and G. F. Pires, 2010: Effects of Amazon and central Brazil deforestation scenarios on the duration of the dry season in the arc of deforestation. *Int. J. Climatol.,* **30,** 1970–1979.

Culf, A., J. L. Esteves, A. O. Marques Filho, and H. R. da Rocha, 1996: Radiation, temperature and humidity over forest and pastures in Amazonia. *Amazonian Deforestation and Climate,* J. Gash, Ed., Institute of Hydrology, 175–192.

D'Almeida, C., C. J. Vörösmarty, G. C. Hurtt, J. A. Marengo, S. L. Dingman, and B. D. Keim, 2007: The effects of deforestation on the hydrological cycle in Amazonia: A review on scale and resolution. *Int. J. Climatol.,* **27,** 633–647.

Dirmeyer, P. A., and K. L. Brubaker, 2007: Characterization of the global hydrologic cycle from a back-trajectory analysis of atmospheric water vapor. *J. Hydrometeor.,* **8,** 20–37.

——, C. A. Schlosser, and K. L. Brubaker, 2009: Precipitation, recycling, and land memory: An integrated analysis. *J. Hydrometeor.,* **10,** 278–288.

Fisch, G., and Coauthors, 2004: The convective boundary layer over pasture and forest in Amazonia. *Theor. Appl. Climatol.,* **78,** 47–59.

Foley, J. A., and Coauthors, 2007: Amazonia revealed: Forest degradation and loss of ecosystem goods and services in the Amazon basin. *Front. Ecol. Environ,* **5,** 25–32.

Friedl, M., and Coauthors, 2002: Global land cover mapping from MODIS: Algorithms and early results. *Remote Sens. Environ.,* **83,** 287–302.

Gash, J., and C. Nobre, 1997: Climatic effects of Amazonian deforestation: Some results from ABRACOS. *Bull. Amer. Meteor. Soc.,* **78,** 823–830.

Grimm, A. M., 2010: Interannual climate variability in South America: Impacts on seasonal precipitation, extreme events, and possible effects of climate change. *Stochastic Environ. Res. Risk Assess.,* **25,** 537–554.

——, S. E. T. Ferraz, and J. Gomes, 1998: Precipitation anomalies in southern Brazil associated with El Niño and La Niña events. *J. Climate,* **11,** 2863–2880.

Harding, K. J., and P. K. Snyder, 2012: The atmospheric response to irrigation in the Great Plains. Part II: The precipitation of

irrigated water and changes in precipitation recycling. *J. Hydrometeor.,* **13,** 1687–1703.

Hong, S.-B., V. Lakshmi, E. E. Small, F. Chen, M. Tewari, and K. W. Manning, 2009: Effects of vegetation and soil moisture on the simulated land surface processes from the coupled WRF/Noah model. *J. Geophys. Res.,* **114,** D18118, doi:10.1029/2008JD011249.

Hong, S.-Y., and J.-O. J. Lim, 2006: The WRF Single-Moment 6-Class Microphysics Scheme (WSM6). *J. Korean Meteor. Soc.,* **42,** 129–151.

Huete, A. R., and Coauthors, 2006: Amazon rainforests green-up with sunlight in dry season. *Geophys. Res. Lett.,* **33,** L06405, doi:10.1029/2005GL025583.

Huntingford, C., and Coauthors, 2013: Simulated resilience of tropical rainforests to CO_2-induced climate change. *Nat. Geosci.,* **6,** 268–273.

Kanamitsu, M., W. Ebisuzaki, J. Woollen, S.-K. Yang, J. J. Hnilo, M. Fiorino, and G. L. Potter, 2002: NCEP–DOE AMIP-II Reanalysis (R-2). *Bull. Amer. Meteor. Soc.,* **83,** 1631–1643.

Lee, J., B. R. Lintner, C. K. Boyce, and P. J. Lawrence, 2011: Land use change exacerbates tropical South American drought by sea surface temperature variability. *Geophys. Res. Lett.,* **38,** L19706, doi:10.1029/2011GL049066.

Lee, S., and E. H. Berbery, 2012: Land cover change effects on the climate of the La Plata basin. *J. Hydrometeor.,* **13,** 84–102.

Lewis, S. L., P. M. Brando, O. L. Phillips, G. M. F. Van Der Heijden, and D. Nepstad, 2011: The 2010 Amazon drought. *Science,* **331,** 554.

Malhi, Y., J. T. Roberts, R. A. Betts, T. J. Killeen, W. Li, and C. A. Nobre, 2008: Climate change, deforestation, and the fate of the Amazon. *Science,* **319,** 169–172.

Marengo, J. A., 2004: Interdecadal variability and trends of rainfall across the Amazon basin. *Theor. Appl. Climatol.,* **78,** 79–96.

——, and Coauthors, 2008: The drought of Amazonia in 2005. *J. Climate,* **21,** 495–516.

——, J. Tomasella, L. M. Alves, W. R. Soares, and D. A. Rodriguez, 2011: The drought of 2010 in the context of historical droughts in the Amazon region. *Geophys. Res. Lett.,* **38,** L12703, doi:10.1029/2011GL047436.

Medvigy, D., R. L. Walko, and R. Avissar, 2011: Effects of deforestation on spatiotemporal distributions of precipitation in South America. *J. Climate,* **24,** 2147–2163.

Morton, D. S., and Coauthors, 2006: Cropland expansion changes deforestation dynamics in the southern Brazilian Amazon. *Proc. Natl. Acad. Sci. USA,* **103,** 14 637–14 641.

NASA, cited 2006: Monthly 0.25° × 0.25° merged TRMM and other sources rainfall. [Available online at http://mirador.gsfc.nasa.gov/cgi-bin/mirador/presentNavigation.pl?tree=project&project=TRMM&dataGroup=Gridded&dataset=3B43:%20Monthly%200.25%20x%200.25%20degree%20merged%20TRMM%20and%20other%20sources%20estimates&version=006.]

Nepstad, D. C., and Coauthors, 1994: The role of deep roots in the hydrological and carbon cycles of Amazonian forests and pastures. *Science,* **372,** 666–669.

Nobre, C. A., G. O. Obregón, J. A. Marengo, R. Fu, and G. Poveda, 2009: Characteristics of Amazonian climate: Main features. *Amazonia and Global Change, Geophys. Monogr.,* Vol. 186, Amer. Geophys. Union, 149–162.

Phillips, O. L., and Coauthors, 2009: Drought sensitivity of the Amazon rainforest. *Science,* **323,** 1344–1347.

Ramankutty, N., and J. Foley, 1999: Estimating historical changes in global land cover: Croplands from 1700 to 1992. *Global Biogeochem. Cycles,* **13,** 997–1027.

——, A. T. Evan, C. Monfreda, and J. A. Foley, 2008: Farming the planet: 1. Geographic distribution of global agricultural lands in the year 2000. *Global Biogeochem. Cycles,* **22,** GB1003, doi:10.1029/2007GB002952.

Saatchi, S., S. Asefi-Najafabady, Y. Malhi, L. E. O. C. Aragão, L. O. Anderson, R. B. Myneni, and R. Nemani, 2012: Persistent effects of severe drought on Amazonian forest canopy. *Proc. Natl. Acad. Sci. USA,* **110**, 565–570, doi:10.1073/pnas.1204651110.

Sahin, V., and M. J. Hall, 1996: The effects of afforestation and deforestation on water yields. *J. Hydrol.,* **178,** 293–309.

Saleska, S. R., K. Didan, A. R. Huete, and H. R. Da Rocha, 2007: Amazon forests green-up during 2005 drought. *Science,* **318,** 612.

Skamarock, W. C., and Coauthors, 2008: A description of the Advanced Research WRF version 3. NCAR Tech. Note NCAR/TN-475+STR, 113 pp. [Available online at http://www.mmm.ucar.edu/wrf/users/docs/arw_v3.pdf.]

Snyder, P., 2010: The influence of tropical deforestation on the Northern Hemisphere climate by teleconnections. *Earth Interact.,* **14,** doi:10.1175/2010EI280.1.

——, C. Delire, and J. A. Foley, 2004: Evaluating the influence of different vegetation biomes on the global climate. *Climate Dyn.,* **23,** 279–302.

Soares-Filho, B. S., and Coauthors, 2006: Modelling conservation in the Amazon basin. *Nature,* **440,** 520–523.

Toomey, M., D. A. Roberts, C. Still, M. L. Goulden, and J. P. McFadden, 2011: Remotely sensed heat anomalies linked with Amazonian forest biomass declines. *Geophys. Res. Lett.,* **38,** L19704, doi:10.1029/2011GL049041.

van der Ent, R. J., H. H. G. Savenije, B. Schaefli, and S. C. Steele-Dunne, 2010: Origin and fate of atmospheric moisture over continents. *Water Resour. Res.,* **46,** W09525, doi:10.1029/2010WR009127.

von Randow, C., and Coauthors, 2004: Comparative measurements and seasonal variations in energy and carbon exchange over forest and pasture in south west Amazonia. *Theor. Appl. Climatol.,* **78,** 5–26.

Walker, R., and Coauthors, 2009: Protecting the Amazon with protected areas. *Proc. Natl. Acad. Sci. USA,* **106,** 10 582–10 586.

Xu, L., A. Samanta, M. H. Costa, S. Ganguly, R. R. Nemani, and R. B. Myneni, 2011: Widespread decline in greenness of Amazonian vegetation due to the 2010 drought. *Geophys. Res. Lett.,* **38,** L07402, doi:10.1029/2011GL046824.

Yoon, J. H., and N. Zeng, 2010: An Atlantic influence on Amazon rainfall. *Climate Dyn.,* **34,** 249–264.